



THE UNIVERSITY *of* EDINBURGH

Edinburgh Research Explorer

Solar light and metal-doped TiO₂ to eliminate water-transmitted bacterial pathogens

Citation for published version:

Venieri, D, Fraggadaki, A, Kostadima, M, Chatzisyneon, E, Binas, V, Zachopoulos, A, Kiriakidis, G & Mantzavinos, D 2014, 'Solar light and metal-doped TiO₂ to eliminate water-transmitted bacterial pathogens: Photocatalyst characterization and disinfection performance' Applied Catalysis B: Environmental, vol. 154-155, pp. 93-101. DOI: 10.1016/j.apcatb.2014.02.007

Digital Object Identifier (DOI):

[10.1016/j.apcatb.2014.02.007](https://doi.org/10.1016/j.apcatb.2014.02.007)

Link:

[Link to publication record in Edinburgh Research Explorer](#)

Document Version:

Peer reviewed version

Published In:

Applied Catalysis B: Environmental

General rights

Copyright for the publications made accessible via the Edinburgh Research Explorer is retained by the author(s) and / or other copyright owners and it is a condition of accessing these publications that users recognise and abide by the legal requirements associated with these rights.

Take down policy

The University of Edinburgh has made every reasonable effort to ensure that Edinburgh Research Explorer content complies with UK legislation. If you believe that the public display of this file breaches copyright please contact openaccess@ed.ac.uk providing details, and we will remove access to the work immediately and investigate your claim.



1 **Applied Catalysis B: Environmental. 154-155, p. 93-101 9 p.**

2

3 **Solar light and metal-doped TiO₂ to eliminate water-transmitted bacterial**
4 **pathogens: Photocatalyst characterization and disinfection performance**

5

6 Danae Venieri^{a*}, Antonia Fraggadaki^a, Maria Kostadima^a, Efthalia Chatzisyneon^{a†}, Vasilios
7 Binas^b, Apostolos Zachopoulos^b, George Kiriakidis^{b, c}, Dionissios Mantzavinos^d

8

9 ^a School of Environmental Engineering, Technical University of Crete, GR-73100 Chania,
10 Greece.

11 ^b Institute of Electronic Structure and Laser (IESL), FORTH, Vasilika Vouton, GR-70013
12 Heraklion, Greece.

13 ^c Department of Physics, University of Crete, GR-70013 Heraklion, Greece.

14 ^d Department of Chemical Engineering, University of Patras, Caratheodory 1, University
15 Campus, GR-26504 Patras, Greece.

16

* Corresponding author. Tel: +302821037801; E-mail address: danae.venieri@enveng.tuc.gr

† Current address: Institute for Infrastructure and Environment, School of Engineering, The University of Edinburgh, The King's Buildings, Edinburgh EH9 3JL, United Kingdom.

17 **Abstract**

18 The present study deals with the inactivation of *Escherichia coli* and *Klebsiella pneumoniae*
19 in water by means of heterogeneous photocatalysis under simulated solar irradiation. For this
20 purpose, novel Mn-, Co- and Mn/Co-doped TiO₂ catalysts were prepared. A straightforward,
21 simple and inexpensive process has been developed based on a co-precipitation method for
22 the synthesis of metal-doped catalysts, which were subsequently assessed in terms of their
23 disinfection efficiency. The effect of various operating conditions, such as metal dopant (Mn-,
24 Co- and Mn/Co), dopant concentration (0.02-1 wt%), catalyst concentration (25-250 mg/L),
25 bacterial concentration (10²-10⁸ CFU/mL), treatment time (up to 60 min), toxic effects on
26 bacteria and photon flux (4.93-5.8×10⁻⁷ einstein/(L.s)), was examined under simulated solar
27 irradiation. Metal-doped TiO₂ samples were prepared reproducibly and doping shifted the
28 optical absorption edge to the visible region. Their activity was superior to the respective of
29 commercially available P25 titania. The reference strains of *E. coli* and *K. pneumoniae* proved
30 to be readily inactivated during photocatalytic treatment of aqueous samples, since
31 disinfection occurred rapidly (i.e. after only 10 min of irradiation) with the dopant
32 concentration affecting the overall process to a certain extent. Disinfection follows a pseudo-
33 first order kinetic rate in terms of both bacteria removal. Inactivation of the bacteria is
34 attributed to the oxidative degradation of their cells and increase of their cell permeability and
35 not to the potential toxicity of the metal-doped semiconductors, which did not exhibit any
36 bactericidal properties. It has been shown that the improved activity of the Mn-, Co-, and
37 binary Mn/Co doped TiO₂ is accredited to the fact that they can be activated in the visible part
38 of the spectrum, in the absence of UV light (i.e. >420 nm).

39

40 **Keywords:**

41 Water disinfection; metal doping; solar photocatalysis; *E. coli*; *K. pneumoniae*

42 **1. Introduction**

43

44 Occurrence of bacterial pathogens and faecal contamination in surface water may pose
45 high health risks, as they are considered major agents of waterborne diseases. Given that
46 potable water is an essential requirement, efficiency of disinfection techniques is imperative
47 for the adequate inactivation of microorganisms and the protection of public health [1]. The
48 most popular disinfection techniques nowadays involve chemical compounds, filtration or
49 radiation (e.g. chlorination, ozonation, UV irradiation etc.), which may act by different means
50 like inhibition of enzymatic activity or destruction of cellular components [2]. However,
51 considerable disadvantages including toxic by-products generated during chlorination, high
52 cost of ozonation and action limitation depending on source-water turbidity when UV
53 irradiation is applied, have led to the development of alternative methods [3, 4].

54 Semiconductor photocatalysis has emerged as a promising technique for microbial
55 inactivation in various aqueous matrices, including diverse types of bacteria, fungi, viruses,
56 and spores [5-7]. Titanium dioxide (TiO_2) is widely used as a photocatalyst in these processes
57 due to its high efficiency, low toxicity, physico-chemical stability and low cost [2, 6, 8, 9]. A
58 drawback, regarding most commercially available TiO_2 catalysts, is that they are mainly
59 active under UV spectral range because of the high required band gap energy (~ 3.2 eV) for
60 excitation of the semiconductor. Therefore, the bactericidal potential of TiO_2 photocatalysis
61 has been extensively studied with the use of UV light, which is a small fraction of the total
62 solar-light spectrum, excluding solar source of energy, which is abundant and free of cost [5,
63 10-12].

64 For this purpose, over the last decade, research interest has been focused on the use of solar
65 irradiation for photocatalysis and thus the exploitation of the visible light energy. The
66 photocatalytic efficiency of TiO_2 has been improved by many different strategies, which have

67 been adopted for either morphological or chemical modifications of the catalyst [2, 8, 13].
68 The latter involve incorporation of additional components in the TiO₂ structure, like non-
69 metal or/and noble and transition metal deposition. Doping the TiO₂ by several metals such as
70 copper, cobalt, manganese, etc. broadens the absorption spectrum of these semiconductors
71 towards the visible light region, as new energy levels are formed between the valence and
72 conduction band [1, 12-19]. The nature and the amount of the doping agent usually play an
73 important role concerning the photocatalytic activity. On the other hand, some possible
74 limitations have been reported like photo-induced corrosion and promoted charge
75 recombination at some metal sites [2, 8, 20].

76 Up until now, various studies have been conducted in terms of the evaluation of
77 disinfection efficiency of doped catalysts during water treatment under visible light, using
78 mostly *Escherichia coli* as a model microorganism [3-5, 10, 14, 16, 18, 21-24]. In most cases,
79 inactivation of bacteria has been attributed to the decomposition of bacterial outer membrane
80 due to phospholipid peroxidation of the membrane, caused primarily by hydroxyl radicals,
81 generated during treatment [25-27]. Apart from *E. coli*, the information regarding the
82 behaviour of other bacteria is very limited. The bacterial content of water consists of many
83 groups and species, which exhibit variable tolerance in disinfection as a result of differences
84 in cellular structure. *Klebsiella pneumoniae* is considered as an emerging human pathogen
85 and can be transmitted through water consumption, but it has been merely studied as far as its
86 resistance against disinfection is concerned [28, 29].

87 In this perspective, the objectives of the present work were (i) to prepare novel cobalt- and
88 manganese-doped titania materials and investigate their structural properties, and (ii) to study
89 their potential to purify aqueous samples in terms of *E. coli* and *K. pneumoniae* reference
90 strains removal under solar radiation. For this purpose, several operating parameters were
91 investigated, namely catalyst type and loading, dopant concentration, initial bacterial

92 concentration, as well as photon flux, which typically influence disinfection effectiveness.
93 Furthermore, scanning electron microscopy (SEM) was employed to detect destruction of
94 cellular structure induced by photocatalysis.

95

96 **2. Experimental**

97

98 *2.1 Materials*

99 Titanium (IV) oxysulfate hydrate ($\text{TiOSO}_4 \cdot x\text{H}_2\text{O}$), manganese (II) acetate tetrahydrate
100 ($\text{Mn}(\text{CH}_3\text{COO})_2$), cobalt (II) acetate tetrahydrate ($\text{Co}(\text{CH}_3\text{COO})_2$) and ammonium hydroxide
101 (25% NH_4OH) purchased from Aldrich were applied. Commercially available titanium
102 dioxide (TiO_2 P25) was purchased from Degussa - Evonik Corp. (physicochemical
103 characteristics are anatase:rutile 75:25, particle size of 21 nm and BET area of $50 \text{ m}^2/\text{g}$) and
104 was used as benchmark.

105

106 *2.2 Preparation of metal-doped TiO_2*

107 A co-precipitation method was used to prepare metal-doped TiO_2 nanoparticles with molar
108 ratio in different concentrations in the range of 0.02 - 1 wt%. Doped titanium dioxide was
109 precipitated at pH ~ 7 from aqueous solution of TiOSO_4 titanium (IV) oxysulfate hydrate and
110 dopant (Mn or Co or Mn/Co) by the addition of ammonia. After aging the suspension
111 overnight, the precipitate was filtered and dried under air at 373K. The residue was crushed to
112 a fine powder and calcined in a furnace at 973 K for 3 h. More details can be found in
113 previous work [13].

114

115 *2.3 Catalyst characterization techniques*

116 Powder X-ray diffraction patterns were collected on a Rigaku D/MAX-2000H rotating
117 anode diffractometer (CuK α radiation) equipped with the secondary pyrolytic graphite
118 monochromator operated at 40 kV and 80 mA over the 2θ collection range of 10–80°. The
119 scan rate was 0.05° s⁻¹. The average particle size (D in nm) of nanoparticles was calculated
120 from the line broadening of the X-ray diffraction peak according to the Scherrer formula, as
121 follows:

$$122 \quad D = k\lambda/(\beta\cos\theta) \quad (1)$$

123 where k is the shape factor (~ 0.9), λ is the wavelength of the X-ray radiation (1.54 Å for
124 CuK α), β is the full width at half maximum (FWHM) of the diffraction peak measured at 2θ ,
125 and θ is the Bragg angle.

126 The phase content of TiO₂ samples was calculated using the formula:

$$127 \quad \%f_A = [1/(1+1.265 \times I_R/I_A)] \times 100 \quad (2)$$

128 where f_A is the content of anatase, and I_A and I_R are the integrated intensities of the anatase
129 (100) and rutile (110) peaks respectively.

130 The UV – Visible diffuse reflectance spectra of the final powders were measured on a
131 Perkin Elmer LAMBDA 950 with BaSO₄, as reference standard. The diffuse reflectance
132 spectra were plotted as the Kubelka – Munk function, $F(R)$, versus wavelength based on the
133 Kubelka – Munk equation:

$$134 \quad F(R) = (1-R)^2/(2R) \quad (3)$$

135 where the reflectance $R = R_{\text{sample}}/R_{\text{reference}}$. The band gaps were then determined from the
136 Kubelka – Munk function and the Tauc plots.

137 Surface morphology and elemental analysis of the samples were carried out using scanning
138 electron microscopy (SEM) and an energy dispersive spectrometer (EDS) on a JSM-6390LV
139 instrument. The microscopic nanostructures were studied by transmission electron
140 microscopy (TEM) working at 200kV (JEM-2100 instrument equipped with LaB6 filament).

141

142 2.4 Disinfection experiments

143 The bacterial strains used in the present study were *E. coli* ATCC 23716 (American Type
144 Culture Collection, Rockville, Md. USA) and *K. pneumoniae* NCTC 5056 (Public Health
145 England Culture Collections). Both reference strains were inoculated separately in 10 mL of
146 nutrient broth (HiMedia Laboratories) and grown overnight at 37°C. The concentration of
147 bacterial cells in the suspension was estimated measuring its optical density at 600 nm
148 (Shimadzu UV1240 spectrophotometer) where, according to McFarland scale, an absorbance
149 of 0.132 corresponds approximately to a cell density of 1.5×10^8 CFU/mL. Plate counts were
150 also performed for accurate bacterial count. In each case, suspensions were properly diluted to
151 achieve the desired initial bacterial concentration, which was used for the subsequent
152 experiments.

153 Photocatalytic experiments were conducted in batch type, laboratory scale photoreactor.
154 Solar irradiation experiments were carried out in a solar radiation simulator system (Newport,
155 model 96000) equipped with a 150 W xenon ozone-free lamp and an Air Mass 1.5 Global
156 Filter (Newport, model 81094), simulating solar radiation reaching the surface of the earth at
157 a zenith angle of 48.2°. According to the spectral irradiance data given by the manufacturer,
158 simulated solar radiation contains about 5% UV-A radiation, and 0.1% UV-B radiation, while
159 the filter cuts radiations with wavelengths lower than 280 nm. The incident radiation intensity
160 on the photochemical reactor in the UV region of the electromagnetic spectrum was measured
161 actinometrically using 2-nitrobenzaldehyde (Sigma-Aldrich) as the chemical actinometer [30,
162 31] and it was found to be 5.8×10^{-7} einstein/(L.s), which corresponds to an irradiance of
163 1.31×10^{-2} W/m². Additional runs were performed with (i) a 420 nm cutoff filter to remove all
164 the UV light (FSQ-GG420, 50.8 mm x 50.8 mm), (ii) filter (FSQ-ND02, 50.8 mm×50.8 mm,
165 80% transmittance at 632.8 nm) to reduce irradiance to 5.3×10^{-7} einstein/(L.s), and (iii) filter

166 (FSQ-ND04, 50.8 mm×50.8 mm, 40% transmittance at 632.8 nm) to reduce irradiance to 4.93
167 10^{-7} einstein/(L.s). Reactions took place in an open, double-walled, cylindrical glass vessel
168 under continuous stirring.

169 In a typical run, the bacteria suspension was spiked in sterile water of 200 mL which were
170 then loaded in the reaction vessel with the appropriate amount of catalyst. The solution was
171 left in the dark under stirring for 20 min in order to equilibrate and then exposed to solar
172 irradiation; this moment was taken as the starting point (time zero) of the disinfection
173 experiment. Temperature was maintained at $25\pm 2^{\circ}\text{C}$ with a temperature control unit. The
174 external reaction vessel was covered with aluminum foil to reflect irradiation exerting the
175 outer wall of the reaction vessel. At specific time intervals samples of about 1.5 mL of the
176 reaction solution were withdrawn and analyzed with respect to viable bacterial cells applying
177 conventional culture method. All disinfection experiments were performed in triplicate.

178 Disinfection rate was measured in terms of *E. coli* and *K. pneumoniae* inactivation. The
179 detection and enumeration of both bacteria in the solution were performed using the serial
180 dilution streak plate procedure. The media used in the study were HiCrome Coliform Agar
181 (HiMedia Laboratories) and M-FC agar M1124 (HiMedia Laboratories) for *E. coli* and *K.*
182 *pneumonia*, respectively. Incubation was performed at 37°C for 20-24 h before viable counts
183 were determined.

184 SEM observation of bacterial cells was carried out before and after treatment in each case,
185 with the view to detect any destruction of cellular structure of reference strains induced by
186 photocatalysis.

187

188 **3. Results and discussion**

189

190 *3.1. Structural and optical properties of metal-doped TiO₂ nanoparticles*

191 The XRD patterns of Mn-, Co-doped TiO₂, and binary Mn/Co co-doped TiO₂ with dopant
192 concentrations in the solution ranging from 0.02 to 1% for Mn- and Co-doped and 0.04 to
193 0.1% for the binary Mn/Co co-doped, respectively, calcined at 700°C for 3 h, are shown in
194 Figure 1. Peak at 25.3° corresponds to the crystal plane 101 of the anatase phase. When the
195 dopant concentration was in the range of 0.02 - 0.3 wt% the samples were monophasic with
196 only the anatase polymorph TiO₂ being detected. Catalysts with 1 wt% of Mn- and Co-
197 dopants, respectively exhibited a mixture of phases with both anatase and rutile. The peaks at
198 2θ values of 25.3, 37.6, 48.2, 53.9, 54.8, 62.7 and 75.2 corresponding to the (101), (004),
199 (200), (105), (211), (204) and (215) planes, respectively are all anatase signature peaks. No
200 obvious diffraction peaks attributed to MnO₂ or CoO₂ were observed at low dopants
201 concentrations. Results of the particle size and phase content are shown in Table 1.

202 Figure 2 shows the UV-VIS absorption as a function of wavelength for metal-doped
203 catalysts. Dopants at different concentrations caused considerable absorption shifts towards
204 the visible range (400-800 nm) in comparison to the absorption threshold of P25 at 400 nm.
205 Moreover, increasing the dopant concentration led to a significant decrease in the band gap
206 energy below the value of 3.2 eV, which is required for excitation of the commercial P25
207 (Table 2). The band gap energy ranged between 2.4 and 2.87 eV and 2.4 and 2.97 eV for Mn
208 and Co-doped catalysts, respectively. In the case of Co and Mn/Co-doped TiO₂, an extra sub-
209 band gap energy was recorded in the range 1.4-1.6 eV, depending on the dopant concentration
210 (Table 2). The new absorption shoulder of these catalysts at 400-800 nm, related to the
211 presence of dopant (Figures 2b and 2c), may play key role in enhancing the overall
212 photocatalytic activity within the visible range. The textural features of the catalysts were
213 investigated with SEM (images are not shown for the sake of brevity); no specific
214 morphology changes were detected, while the spherical shape particles of all the samples
215 demonstrated some degree of agglomeration and the diameter ranged from 0.1 to 40 μm.

216 TEM images of the 1 wt% Mn- and 1 wt% Co-doped TiO₂ nanoparticles (Figure 3) confirmed
217 the agglomeration of nanoparticles with size ranging between 35 and 45 nm, consistent with
218 XRD measurements.

219

220 3.2. Photocatalytic disinfection

221 3.2.1. Effect of catalysts concentration

222 Given that the concentration of catalyst in slurry photocatalytic treatment strongly affects
223 the overall process, preliminary runs were performed with both bacterial reference strains
224 testing different commercial and metal-doped TiO₂ loadings. Tested concentrations were in
225 the range 25-250 mg/L for *E. coli* and 100-250 mg/L for *K. pneumoniae*. Higher loadings
226 were selected for *K. pneumoniae*, since it is a bacillus with a prominent capsule, which
227 prevents cell destruction by bactericidal factors [28]. According to the results, increasing the
228 catalyst loading improved inactivation rates for both microorganisms. In the case of *E. coli*,
229 optimal inactivation rates (approximately 4-Log reduction within 5 min of treatment) were
230 achieved when catalysts loading was 100 mg/L, beyond which disinfection reached a plateau.
231 Generally, increasing the photocatalyst concentration leads in lower penetration of light into
232 the slurry, deteriorating disinfection efficiency [3]. Conversely, higher catalysts concentration
233 was required for satisfactory decrease of *K. pneumoniae* population. In the presence of 250
234 mg/L of various types of TiO₂ that were used in the present study, total bacterial killing was
235 recorded in almost 10 min with an initial bacterial density of 10⁵ CFU/mL. Therefore, all
236 subsequent experiments were conducted using 100 mg/L and 250 mg/L of catalysts for *E. coli*
237 and *K. pneumoniae* treatment, respectively. Optimal catalyst loadings may vary among
238 studies as they depend on many parameters such as photocatalytic reactor geometry, light
239 intensity, type of photocatalytic reactor etc. Apart from the trivial reference of *K. pneumoniae*

240 in photocatalytic studies, inactivation of *E. coli* is usually achieved in the range of loadings
241 used in this work [2, 4, 22].

242

243 3.2.2. Effect of catalyst type

244 Bacterial inactivation was recorded only under solar irradiation, when destruction of the
245 cells occurred. Efficiency of the metal-doped TiO₂ catalysts was assessed during a series of
246 photocatalytic experiments, whose results are shown in Figures 4, 5 and 6. It is observed that
247 Mn- and Co-doped catalysts showed better photocatalytic effectiveness than the commercially
248 available P25, in terms of both bacteria inactivation (Figures 4 and 5). Although P25 TiO₂ is
249 well known for its high photoreactivity due to the slow recombination of the electron-hole
250 pair and large surface area [3], metal dopants improved the activity of catalysts considerably,
251 as bacteria killing took place in almost 10 min of treatment. Moreover, it was observed that
252 increasing the dopant concentration, disinfection efficiency was improved, while an increase
253 beyond 0.3 wt% did not show any significant enhancement of the process.

254 Comparing Mn- and Co-, their effect was dependent of the experimental conditions in
255 question and the type of the specific bacterial reference strains. In the case of *E. coli*, a 6-Log
256 reduction was recorded in 10 min of solar irradiation using 0.1 wt% Mn-doped catalyst.
257 Similar population reduction was achieved in longer treatment period (15 min) and at higher
258 dopant concentration (1 wt%) when TiO₂ was doped with Co. Lower metal quantities than the
259 aforementioned ones proved to be insufficient for total *E. coli* inactivation even after 30 min
260 of treatment. As far as *K. pneumoniae* inactivation is concerned (Figure 6) it is observed that
261 the 0.3 wt% Mn- and 1% Co-doped TiO₂ catalysts showed optimum photocatalytic
262 performance when compared to the others and disinfection took place after only 10 min of
263 treatment. Despite that this specific emerging pathogen is considered persistent during various
264 treatments and disinfection techniques, photocatalysis with metal-doped catalysts seems quite

265 promising, since it may demonstrate complete inactivation in short periods with initial cell
266 densities as high as 10^5 CFU/mL.

267 Findings of the current study highlight the acceleration of disinfection process when metal-
268 doped catalysts are employed. The higher concentrations of Co required is probably attributed
269 to the fact that as a transition metal, it may act as a recombination site for the photo-induced
270 charge carriers thus, lowering the quantum efficiency [8]. Fisher et al., who worked with *E.*
271 *coli* and *Enterococcus faecalis* reported more rapid inactivation of both species in the
272 presence of TiO₂ doped with 1 wt% copper under solar irradiation compared to the respective
273 performed with undoped catalyst [1]. The bacterium-killing efficiency of doped TiO₂ is
274 referred to a quite extended variety of microorganisms, including *Listeria monocytogenes*,
275 *Shigella flexneri*, *Vibrio parahaemolyticus*, *Pseudomonas aeruginosa* and many others,
276 highlighting the advantage of dopants application in photocatalytic treatments [6, 23, 25, 28].

277 In further experiments, Mn/Co co-doped TiO₂ nanoparticles were successfully prepared
278 and their disinfection potential was tested under solar irradiation with *E. coli* and *K.*
279 *pneumoniae* reference strains. Inactivation rates are shown in Figure 6. Co-doped catalysts
280 induced a more rapid total bacterial killing in comparison with those with single metal dopant
281 at respective concentration. Surprisingly, a 5-Log reduction of *K. pneumoniae* population was
282 recorded in 15 min with both co-doped TiO₂, while *E. coli* required 30 min for complete
283 elimination with the highest dopants concentration (0.1 wt%). Similar inactivation rates for *E.*
284 *coli* were observed in a relevant study, where TiO₂ nanoparticles co-doped with N and Ag
285 were used for disinfection under visible light irradiation [32]. In another case, the application
286 of N and S co-doped P25 resulted in a 4-Log *E. coli* inactivation after 90 min of exposure to
287 visible light [33]. According to the general observation, composite dopants can compensate
288 the disadvantages of the individual components, inducing a synergistic effect [2, 8].

289 In order to further investigate the destruction of cellular structure of reference strains
290 induced by photocatalysis, SEM was employed and selective images are shown in Figure 7.
291 During photocatalysis the first oxidative stress is caused to bacteria when the catalyst
292 nanoparticles interact with intact cells. The detrimental effect is expanded towards the
293 cytoplasmic membrane, increasing cell permeability and allowing the outlet of intracellular
294 components, which finally cause cell death [14, 25]. In many cases the resultant change in cell
295 permeability is confirmed by potassium ion (K^+) leakage [34]. In the case of *K. pneumoniae*
296 the remnants of polysaccharide capsules combined with material released from the cell are
297 visible (Figures 7h to 7j). The progressive massive generation of hydroxyl radicals during the
298 process overcomes any protection mechanism of bacterial cells, whose density in reaction
299 mixture decreases with increasing time (Figures 4-6). In the course of treatment inactivation
300 becomes slow, which, according to Vijay et al., is attributed to the protection provided to
301 remaining active cells by metabolites excreted from the destructed ones [4].

302

303 3.2.3. Effect of initial bacterial concentration

304 A series of experiments was carried out to assess bacterial inactivation as a function of
305 initial concentration of the cells in the reaction mixture. In general, an increase in bacterial
306 density led to a decrease in the inactivation. Retardation of disinfection was more
307 pronounced in the case of *E. coli*. For instance, when initial concentrations were 10^4 and 10^6
308 CFU/mL the period for total bacterial killing was 15 and 30 min, respectively, while complete
309 inactivation was not achieved in the presence of higher concentration (10^8 CFU/mL), where
310 residual *E. coli* cells reached a plateau showing an overall decrease of 6 orders of magnitude.
311 The almost same trend was recorded for *K. pneumoniae*, which was inactivated in 10 and 15
312 min when starting concentrations were 10^2 and 10^3 CFU/mL, respectively.

313 Disinfection rates can be fitted satisfactorily to a pseudo-first order kinetic expression, as
314 can be seen in Figure 8; from the slopes of the resulting straight lines kinetic rate constants
315 were calculated at 0.53 ($r^2=0.96$), 0.83 ($r^2=0.92$) and 0.77 min^{-1} ($r^2=0.80$) for initial *E. coli*
316 concentration of 10^4 , 10^6 and 10^8 CFU/mL, respectively. The corresponding values for *K.*
317 *pneumoniae* were 0.43 ($r^2=0.92$), 0.57 ($r^2=0.95$) and 1.08 min^{-1} ($r^2=0.99$) for initial
318 concentration of 10^2 , 10^3 and 10^5 CFU/mL.

319 Usually, the disinfection ability of common techniques is inversely proportional to initial
320 bacterial concentration. However, the required time for total inactivation depends on the
321 tested bacterial species in each case. Residual cells of the reference strains after long
322 treatment periods (> 30min) when high initial densities were employed, may be explained by
323 the survival of a resistant subpopulation as a result of protection by clumping of
324 microorganisms or even by genetically conferred resistance [35].

325

326 *3.3 Why does doping enhance photocatalytic disinfection?*

327 Results of the present study highlight the superiority of metal-doped catalysts compared to
328 P25, in terms of bacterial removal in aqueous samples under simulated solar irradiation. In
329 this respect, an attempt was made to identify the likely reasons for the improved activity of
330 doped catalysts.

331 Firstly, a point of consideration should be the biocidal nature of the metals used for the
332 preparation of catalysts. In some cases, metal-doped catalysts induce cell destruction of
333 bacteria, due to the toxicity of metal ions released into the reaction solution [18]. This may
334 occur even at minute metal concentrations according to the oligodynamic effect [36].
335 Accordingly, in order to assess the instantaneous toxicity of the novel Mn- and Co-doped
336 catalysts to microorganisms during their treatment, a set of experiments was performed in the
337 dark with the catalysts which had the lowest (0.02%) and highest (1%) concentration of metal

338 dopants. The catalyst concentration in the aqueous solution was 250 mg/L and initial bacterial
339 concentration of both reference strains was 10^4 CFU/mL. Bacterial density of *E. coli* and *K.*
340 *pneumoniae* remained stable within the period of the treatment, which lasted almost 1 h. It is
341 clearly shown that the metal-doped catalysts were not toxic to the selected reference strains
342 regarding their short-term toxic effects. Many metals are toxic to microorganisms at micro- or
343 millimolar concentrations, resulting in the development of resistance mechanisms in
344 microbial cells. In the case of cobalt, it is required as a trace element in procaryotes and
345 eucaryotes to fulfill a variety of metabolic functions. At high intracellular concentration the
346 redox active metal ion Co^{2+} is highly toxic [37]. According to our results, no bacterial
347 inactivation was recorded in the presence of both catalysts, indicating that no stress was
348 induced in the cells during their exposure to both metals.

349 Secondly, doping shifted catalyst absorption to the visible region up to 600 nm, as well as
350 decreased the band gap energy as clearly shown in Figure 2 and Table 2. Therefore, it was
351 possible to use the main part of the solar spectrum and surpass one of P25 drawbacks, which
352 is its low activity beyond the range of UV light. To investigate this effect further, experiments
353 were performed using a filter to cut-off UV light below 420 nm. The exclusion of UV light
354 led to a considerable inactivation of bacterial populations, which was more pronounced in the
355 case of *E. coli*. Specifically, in the presence of 0.1 and 1 wt% of Mn- and Co-doped TiO_2 the
356 overall decrease of *E. coli* cells after 30 min of treatment was 74.3% and 94%, respectively
357 (data for *E. coli* and Mn are shown in Figure 9a; for the sake of brevity data with Co are not
358 shown). For the same period of time and with the use of 1 wt% Mn- and Co-doped TiO_2 , the
359 respective inactivation of *K. pneumoniae* reached 28% and 44% (data for *K. pneumoniae* and
360 Co are shown in Figure 9b; for the sake of brevity data with Mn are not shown). Noticeably,
361 the commercial P25 catalyst exhibited no photocatalytic activity above 420 nm and bacterial
362 populations of both strains remained intact throughout the process (data not shown). The

363 metal-doped catalysts (0.1 wt% Mn and 1 wt% Co) showed satisfactory photocatalytic activity
364 within the visible spectral range of the provided irradiation, causing detrimental effects on the
365 bacteria, which partly inactivated the cells in the reaction mixture. Their efficiency was
366 improved with the addition of UV light, as bacterial populations reached zero levels within 10
367 min of treatment. The contribution of UV light to the overall photocatalytic activity is clearly
368 shown in Figure 9 as some experiments were also performed at reduced photon fluxes. Total
369 removal of *E. coli* and *K. pneumoniae* occurred within 10 min only at $5.8 \cdot 10^{-7}$ einstein/(L.s),
370 while three-fold or even longer periods were required to achieve the same inactivation at 5.3
371 10^{-7} and $4.93 \cdot 10^{-7}$ einstein/(L.s). The detrimental effect of decreasing flux to disinfection
372 performance was more pronounced in the case of *K. pneumoniae*, highlighting the resistant
373 nature of the strain.

374 These findings verify the fact that chemical doping may act as a satisfactory means for
375 sensitization of TiO₂ in the visible light region, which is responsible for the enhanced
376 photocatalytic activity recorded in this work. Moreover, dopants on the surface of TiO₂ may
377 act as an electron trap, thus promoting interfacial charge transfer and delaying the
378 recombination of the light-induced electron-hole pair [38], which also leads to enhanced
379 activity.

380

381 **4. Conclusions**

382 The present study focused on solar photocatalytic disinfection with the use of novel cobalt-
383 and manganese-doped titania materials and reference strains of *E. coli* and *K. pneumoniae*.

- 384 - Metal-doped TiO₂ was prepared successfully and doping shifted the optical absorption
385 edge to the visible region.
- 386 - Dopants significantly enhanced (by a factor of 2-3) the photocatalytic activity of TiO₂
387 under solar irradiation, in terms of both bacteria inactivation.

- 388 - Dopants concentrations affected the overall process up to a certain level, while an increase
389 beyond 0.3 wt% did not show significant enhancement of disinfection rates. It is implied
390 that doping levels >0.3 wt% introduce heavy modification of the TiO₂ semiconductor, thus
391 hindering the production/diffusion of charges under light and, consequently, precluding the
392 effective interaction of these charges to inactivate bacteria.
- 393 - Comparing Mn and Co dopants, their performance varied depending on operating
394 parameters, such as the reference strain and the initial bacterial concentration.
- 395 - All catalysts were effective for the removal of *K. pneumoniae*, which is considered as an
396 opportunistic pathogen highly resistant in various water treatments.
- 397 - The improved activity of metal-doped titania is accredited to the optical absorption shifts
398 towards the visible region and to the recombination delay of the electron-hole pair, since
399 metals did not exhibit any bactericidal properties and catalysts were considerably
400 sensitized in the absence of UV light.

401

402 **Acknowledgments**

403 The authors would like to acknowledge Mrs. Alexandra Siakouli - Galanopoulou and Electron
404 Microscopy Laboratory “Vassilis Galanopoulos” of the Department of Biology at University
405 of Crete for help with SEM images.

406

407 **References**

- 408 [1] M.B. Fisher, D.A. Keane, P. Fernández-Ibáñez, J. Colreavy, S.J. Hinder, K.G.
409 McGuigan, S.C. Pillai, *Appl. Catal. B: Environ* 130–131 (2013) 8–13.
- 410 [2] S. Malato, P. Fernández-Ibáñez, M.I. Maldonado, J. Blanco, W. Gernjak, *Catal. Today*
411 147 (2009) 1–59.
- 412 [3] R.P.S. Suri, H.M. Thornton, M. Muruganandham, *Environ. Technol.* 33 (2012) 1651–
413 1659.
- 414 [4] M. Vijay, K. Ramachandran, P.V. Ananthapadmanabhan, B. Nalini, B.C. Pillai, F.
415 Bondioli, A. Manivannan, R.T. Narendhirakannan, *Curr. Appl. Phys.* 13 (2013) 510–
416 516.
- 417 [5] J.G. McEvoy, W. Cui, Z. Zhang, *Catal. Today* 207 (2013) 191–199.
- 418 [6] B. Wang, M.K.H. Leung, X.Y. Lu, S.Y. Chen, *Appl. Energ.* 112 (2013) 1190–1197.
- 419 [7] G. Veréb, L. Manczinger, A. Oszkó, A. Sienkiewicz, L. Forró, K. Mogyorósi, A. Dombi,
420 K. Hernádi, *Appl. Catal. B: Environ.* 129 (2013) 194–201.
- 421 [8] M. Pelaez, N.T. Nolan, S.C. Pillai, M.K. Seery, P. Falaras, A.G. Kontos, P.S.M. Dunlop,
422 J.W.J. Hamilton, J.A. Byrne, K. O’Shea, M.H. Entezari, D.D. Dionysiou, *Appl. Catal.*
423 *B: Environ.* 125 (2012) 331–349.
- 424 [9] D. Dvoranová, V. Brezová, M. Mazúra, M.A. Malati, *Appl. Catal. B: Environ* 37 (2002)
425 91–105.
- 426 [10] H.U. Lee, S.C. Lee, S. Choi, B. Son, S.M. Lee, H.J. Kim, J. Lee, *Chem. Eng. J.* 228
427 (2013) 756–764.
- 428 [11] H. Feng, M.H. Zhang, L.E. Yu, *Appl. Catal. A: Gen.* 413–414 (2012) 238–244.
- 429 [12] Q.R. Deng, X.H. Xia, M.L. Guo, Y. Gao, G. Shao, *Mater. Lett.* 65 (2011) 2051–2054.
- 430 [13] V.D. Binas, K. Sambani, T. Maggos, A. Katsanaki, G. Kiriakidis, *Appl. Catal. B:*
431 *Environ.* 113–114 (2012) 79–86.

- 432 [14] C. Karunakaran, G. Abiramasundari, P. Gomathisankar, G. Manikandan, V. Anandi, J.
433 Colloid Interf. Sci. 352 (2010) 68–74.
- 434 [15] J. Marugán, P. Christensen, T. Egerton, H. Purnama, Appl. Catal. B: Environ. 89 (2009)
435 273–283.
- 436 [16] C. Karunakaran, A. Vijayabalan, G. Manikandan, Res. Chem. Intermed. 39 (2013) 1437–
437 1446.
- 438 [17] N.G. Moustakas, A.G. Kontos, V. Likodimos, F. Katsaros, N. Boukos, D. Tsoutsou, A.
439 Dimoulas, G.E. Romanos, D.D. Dionysiou, P. Falaras, Appl. Catal. B: Environ. 130–131
440 (2013) 14–24.
- 441 [18] M.P. Reddy, A. Venugopal, M. Subrahmanyam, Water Res. 41 (2007) 379–386.
- 442 [19] K.B. Jaimy, S. Ghosh, K.G. Warriar, J. Solid State Chem 196 (2012) 465–470.
- 443 [20] V.C. Papadimitriou, V.G. Stefanopoulos, M.N. Romanias, P. Papagiannakopoulos, K.
444 Sambani, V. Tudose, G. Kiriakidis, Thin Solid Films 520 (2011) 1195–1201.
- 445 [21] G. Veréb, L. Manczinger, G. Bozsó, A. Sienkiewicz, L. Forró, K. Mogyorósi, K.
446 Hernádi, A. Dombi, Appl. Catal. B: Environ. 129 (2013) 566–574.
- 447 [22] L. Rizzo, D. Sannino, V. Vaiano, O. Sacco, A. Scarpa, D. Pietrogiacomì, Appl. Catal. B:
448 Environ. 144 (2014) 369–378.
- 449 [23] M.S. Wong, W.C. Chu, D.S. Sun, H.S. Huang, J.H. Chen, P.J. Tsai, N.T. Lin, M.S. Yu,
450 S.F. Hsu, S.L. Wang, H.H. Chang, Appl. Environ. Microbiol. 72 (2006) 6111–6116.
- 451 [24] C. Karunakaran, A. Vijayabalan, G. Manikandan, P. Gomathisankar, Catal. Commun. 12
452 (2011) 826–829.
- 453 [25] S. Swetha, S.M. Santhosh, R.G. Balakrishna, Photochem. Photobiol. 86 (2010) 1127–
454 1134.
- 455 [26] V.A. Nadtochenko, A.G. Rincon, S.E. Stanca, J. Kiwi, J. Photochem. Photobiol. A-
456 Chem. 169 (2005) 131–137.

- 457 [27] J. Kiwi, V. Nadtochenko, *Langmuir* 21 (2005) 4631–4641.
- 458 [28] R.L. Burke, C.A. Whitehouse, J.K. Taylor, E.B. Selby, *Comparative Med.* 59 (2009)
459 589–597.
- 460 [29] M. Wang, B. Cao, Q. Yu, L. Liu, Q. Gao, L. Wang, L. Feng, *J. Clin. Microbiol.* 46
461 (2008) 3555–3563.
- 462 [30] K.L. Willett, R.A. Hites, *J. Chem. Educ.* 77 (2000) 900–902.
- 463 [31] E.S. Galbavy, K. Ram, C. Cort Anastasio, *J. Photochem. Photobiol. A-Chem.* 209 (2010)
464 186–192.
- 465 [32] P. Wu, R. Xie, K. Imlay, J.K. Shang, *Environ. Sci. Technol.* 44 (2010) 6992–6997.
- 466 [33] J.A. Rengifo-Herrera, E. Mielczarski, J. Mielczarski, N.C. Castillo, J. Kiwi, C. Pulgarin,
467 *Appl. Catal. B: Environ.* 84 (2008) 448–456.
- 468 [34] Z. X. Lu, L. Zhou, Z. L. Zhang, W. L. Shi, Z. X. Xie, H. Y. Xie, D. W. Pang, P. Shen,
469 *Langmuir* 19 (2003) 8765–8768.
- 470 [35] R.M. Maier, I.L. Pepper, C.P. Gerba, *Environmental Microbiology*, second ed.,
471 Academic Press, Elsevier, 2009.
- 472 [36] S. Rtimi, M. Pascu, R. Sanjines, C. Pulgarin, M. Ben-Simon, J.C. Lavanchy, A. Houas, J.
473 Kiwi, *Appl. Catal. B: Environ.* 138–139 (2013) 113–121.
- 474 [37] C. Ranquet, S. Ollagnier-de-Choudens, L. Loiseau, F. Barras, M. Fontecave, *J. Biol.*
475 *Chem.* 282 (2007) 30442–30451.
- 476 [38] W. Wang, J. Zhang, F. Chen, D. He, M. Anpo, *J. Coll. Interf. Sci.* 323 (2008) 182–186.

477 **Table 1.**

478 Average particle size and phase composition for Mn-, Co- and Mn/Co-doped TiO₂ catalyst.

Dopant concentration (molar ratio)	Mn-doped TiO ₂		Co-doped TiO ₂		Mn/Co doped TiO ₂	
	Particle size, (nm)	Phase content, f_A	Particle size, (nm)	Phase content, f_A	Particle size, (nm)	Phase content, f_A
	anatase / rutile	% anatase	anatase / rutile	% anatase	anatase / rutile	% anatase
0.02	38.2 / 0	100	44.3 / 0	100	-	-
0.04	39.4 / 0	100	40.4 / 0	100	-	-
0.1	38.7 / 0	100	40.1 / 0	100	40.1 / 0	100
0.3	40.6 / 0	100	37.5 / 0	100	38.6 / 0	100
1	31.1 / 53	86.5	43.5 / 48.7	50.4	-	-

479

480 **Table 2.**

481 Effect of Mn and Co dopant level on band gap.

Dopant concentration (molar ratio)	Mn-doped TiO₂	Co-doped TiO₂	Mn/Co-doped TiO₂
	Indirect band gap (eV)	Indirect band gap (eV)	Indirect band gap (eV)
0.02	2.7	2.97	
0.04	2.85	2.85 [1.6*]	3 [1.6*]
0.1	2.75	2.83 [1.55*]	2.7 [1.5*]
0.3	2.6	2.7 [1.5*]	
1	2.4	2.4 [1.41*]	

482

483 * Sub-band gap

484

485 **Figure captions**

486 **Figure 1**

487 XRD patterns of a) Mn-doped TiO₂ (0.02-1 wt%), b) Co-doped TiO₂ (0.02-1 wt%) and c) Mn
488 & Co co-doped TiO₂ (binary dopant concentration range: 0.04-0.1 wt%).

489 **Figure 2**

490 UV-Vis absorption of P25 and a) Mn-doped TiO₂ (0.02-1 wt%), b) Co-doped TiO₂ (0.02-1
491 wt%) and c) Mn & Co co-doped TiO₂ (binary dopant concentration range: 0.04-1 wt%).

492 **Figure 3**

493 TEM images of a) Mn-doped TiO₂ (1 wt%) and b) Co-doped TiO₂ (1 wt%).

494 **Figure 4**

495 *E. coli* inactivation in the presence of different Mn- and Co-doped TiO₂ catalysts and the
496 commercially available TiO₂ (P25, Evonik). Catalyst concentration is 100 mg/L.

497 **Figure 5**

498 *K. pneumoniae* inactivation in the presence of different a) Mn- and b) Co-doped TiO₂
499 catalysts and the commercially available TiO₂ (P25, Evonik). Catalyst concentration is 250
500 mg/L.

501 **Figure 6**

502 *E. coli* and *K. pneumoniae* inactivation in the presence of Mn & Co co-doped TiO₂. Catalyst
503 concentration is 100 and 250 mg/L for *E. coli* and *K. pneumoniae* inactivation, respectively.

504 **Figure 7**

505 SEM images of *E. coli* (a-e) and *K. pneumoniae* (f-j) without treatment (negative controls)
506 and after photocatalytic treatment in the presence of metal-doped TiO₂.

507 **Figure 8**

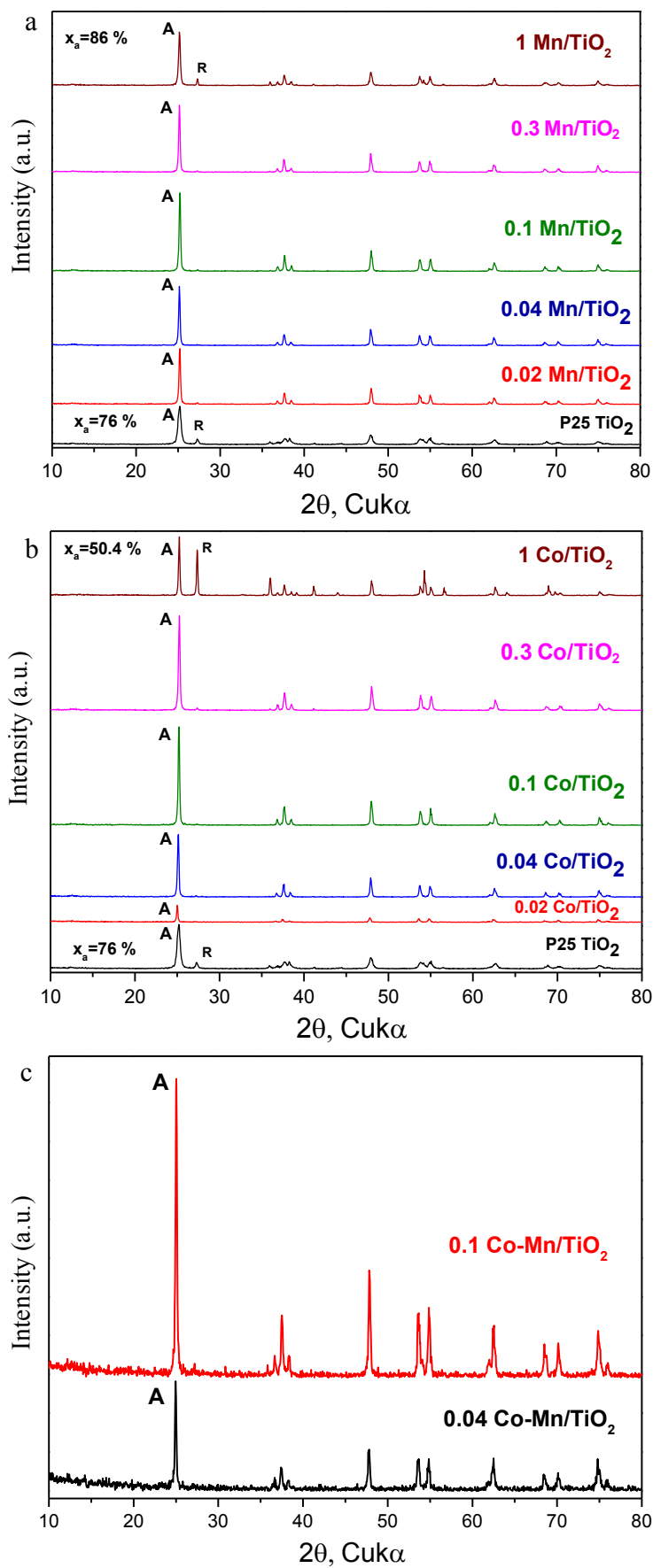
508 Effect of initial bacterial concentration on disinfection efficiency for a) *E. coli* (conditions:
509 0.02 wt% Co, 100 mg/L) and b) *K. pneumoniae* (conditions: 0.3 wt% Mn, 250 mg/L).

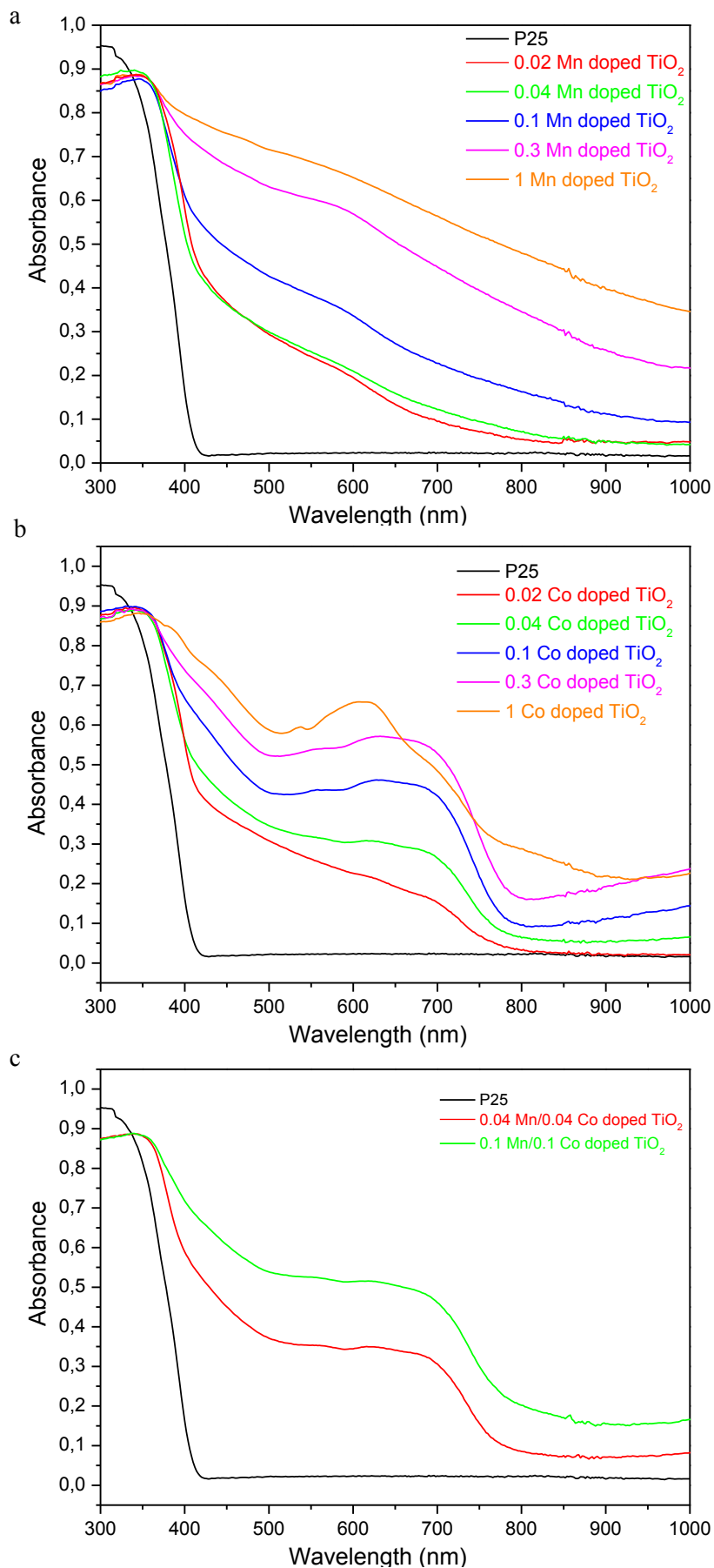
510 **Figure 9**

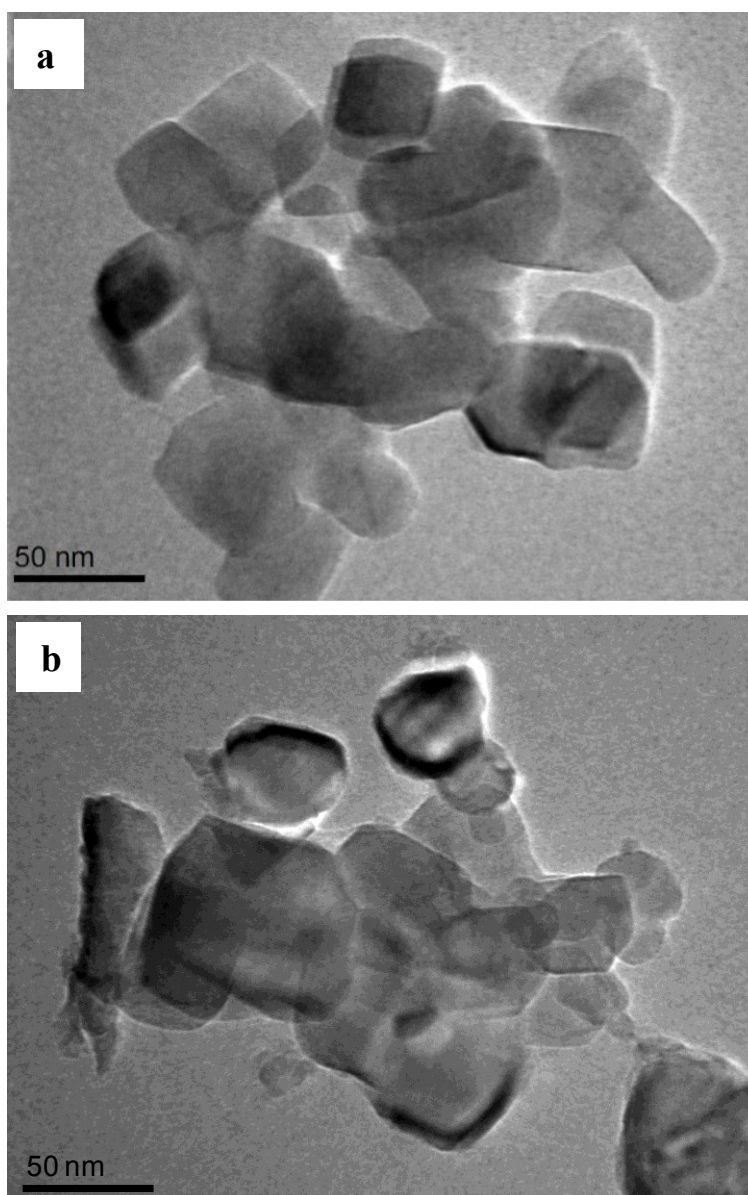
511 Effect of photon flux and wavelength on the inactivation of a) *E. coli* (conditions: 0.1 wt%

512 Mn, 100 mg/L) and b) *K. pneumoniae* (conditions: 1 wt% Co, 250 mg/L).

513



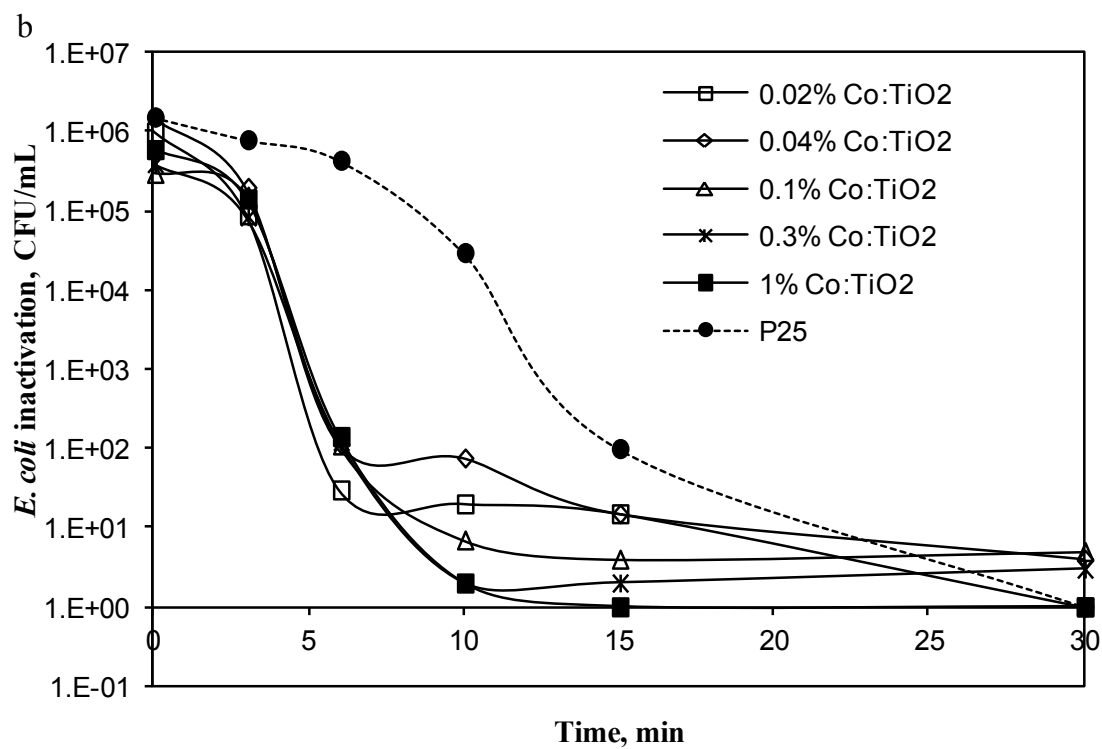
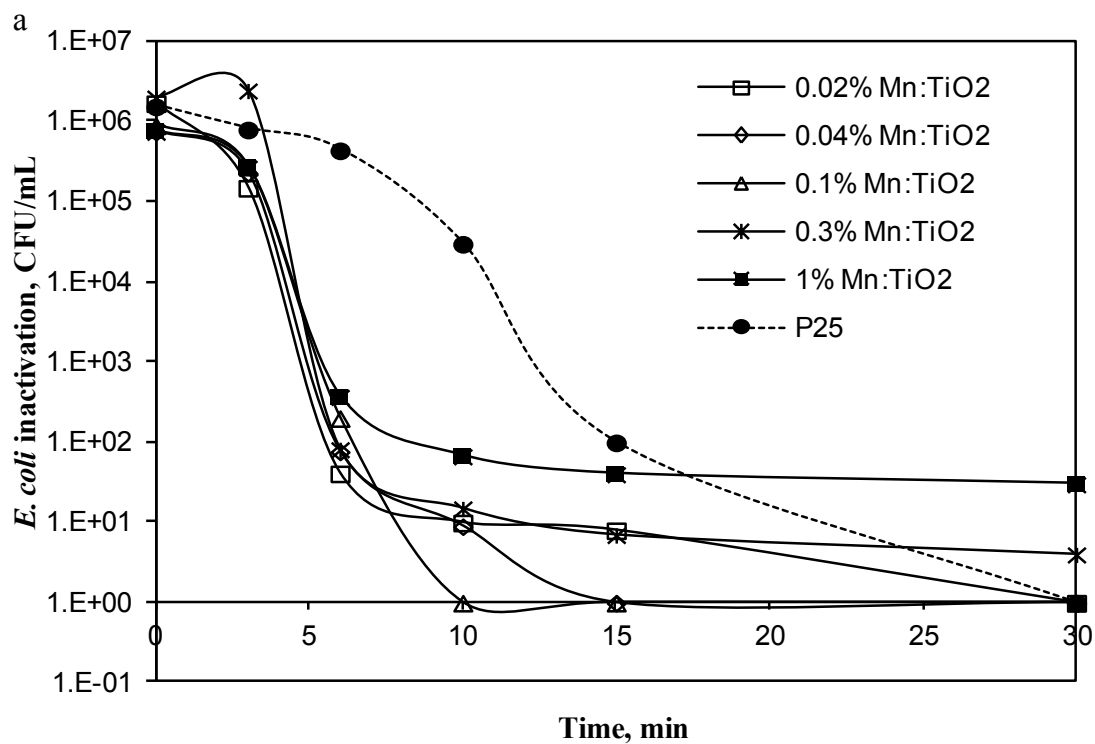




520

521

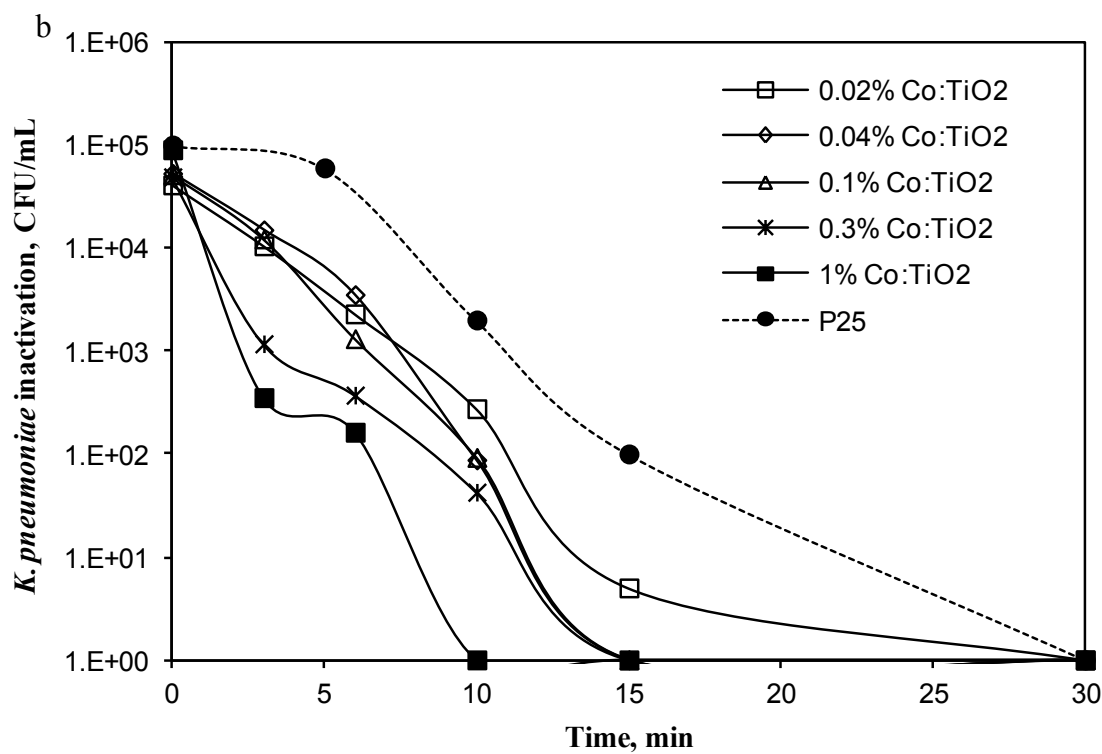
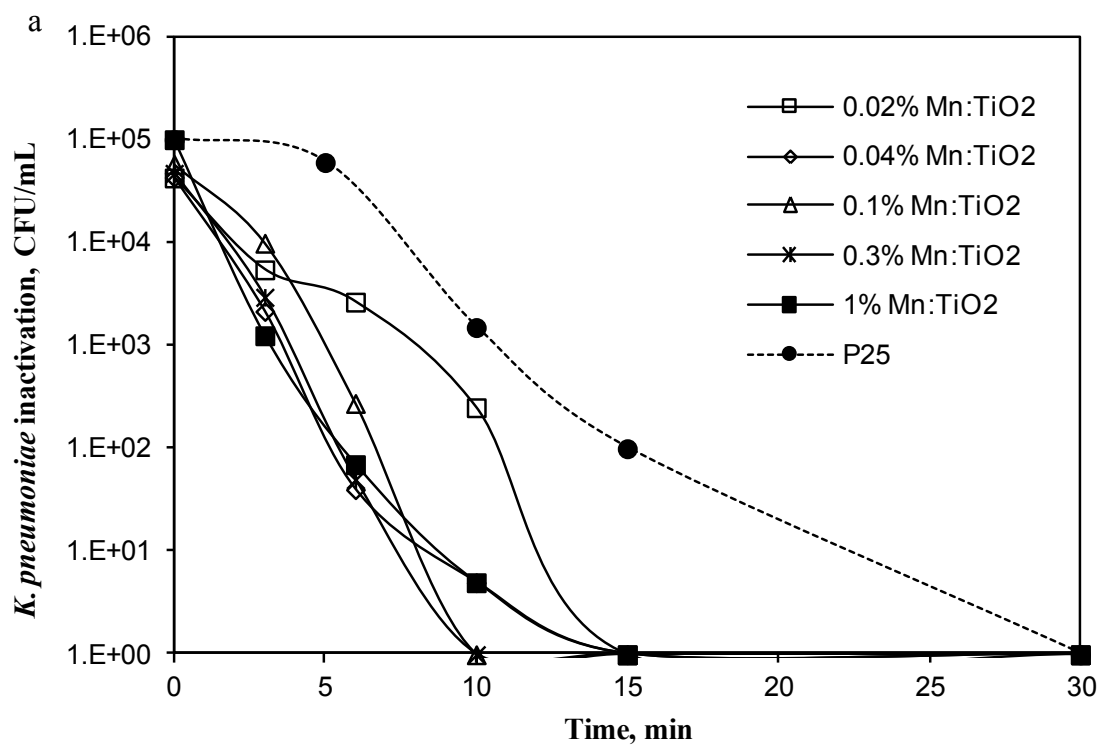
522 **Figure 4**



523

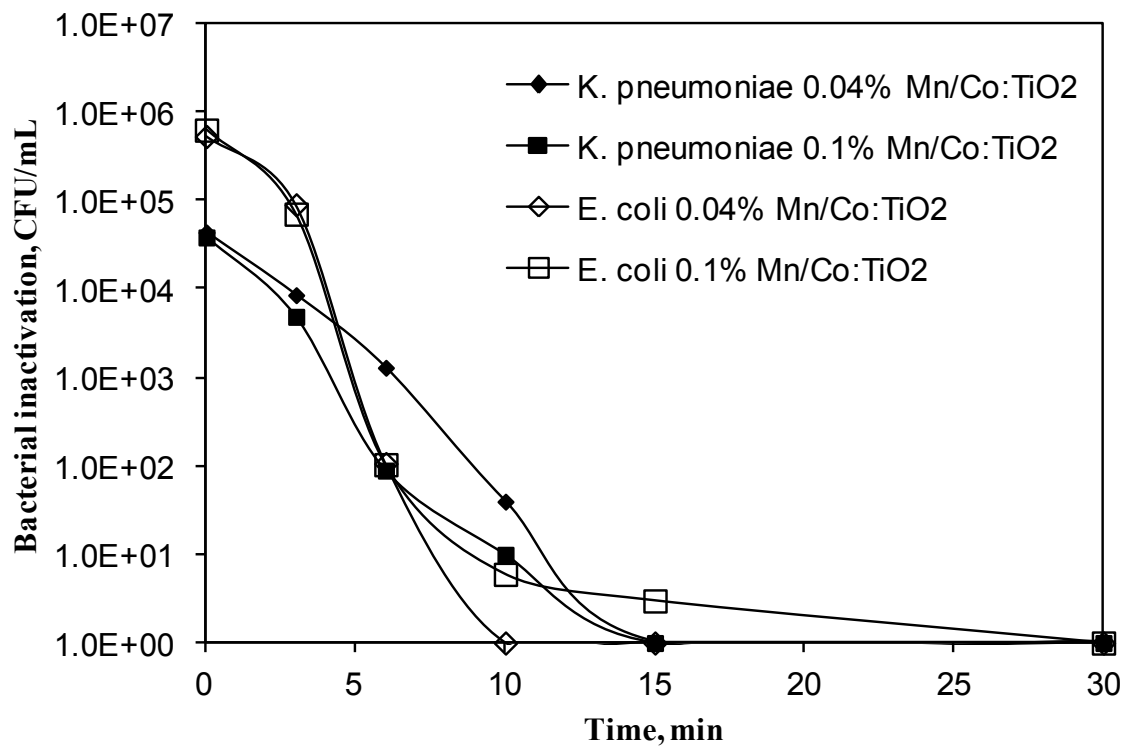
524

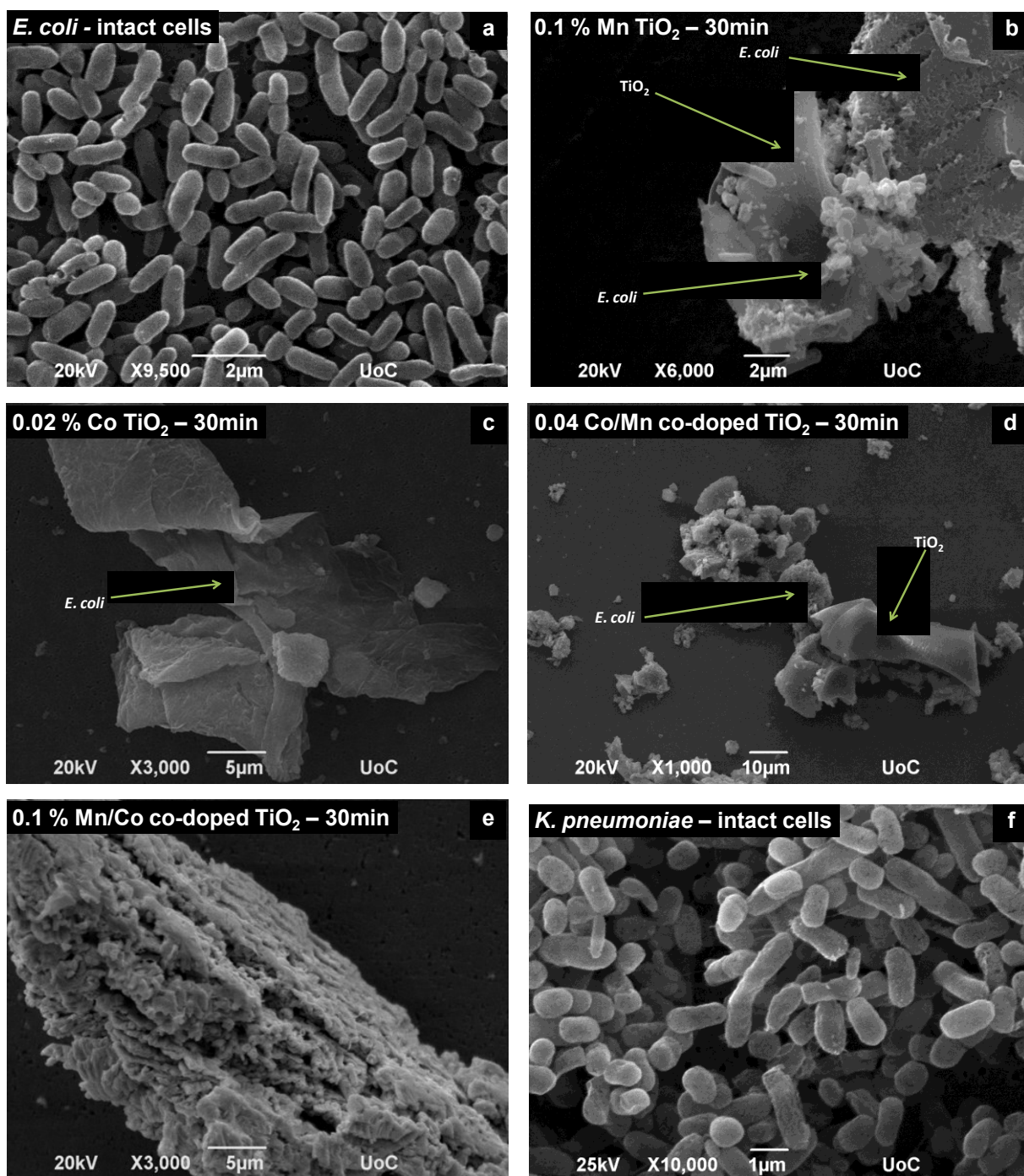
525 **Figure 5**

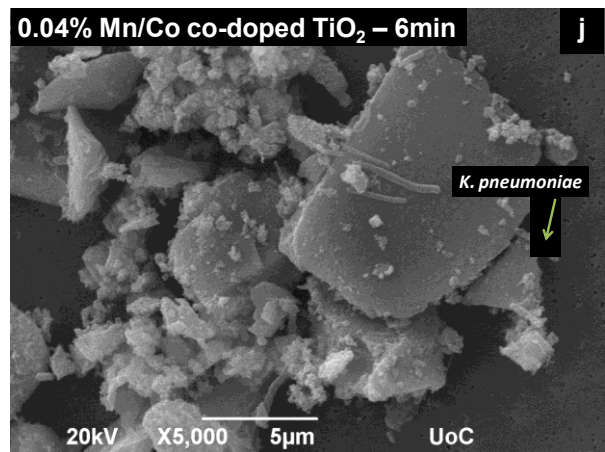
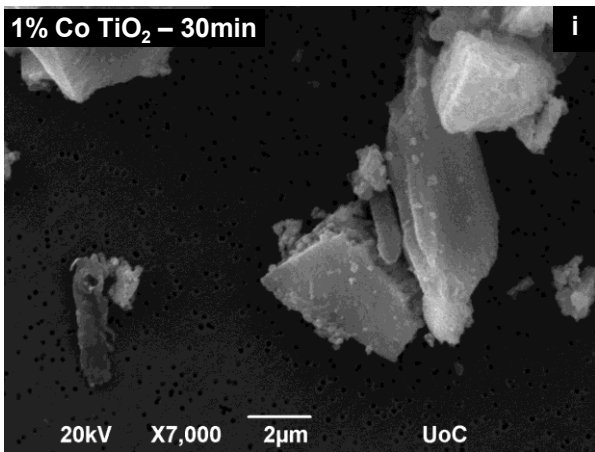
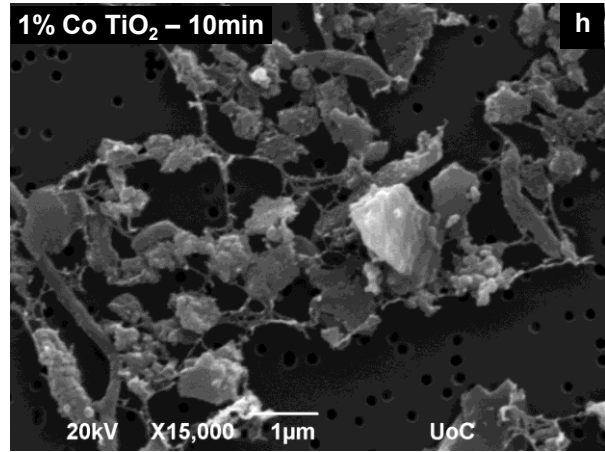
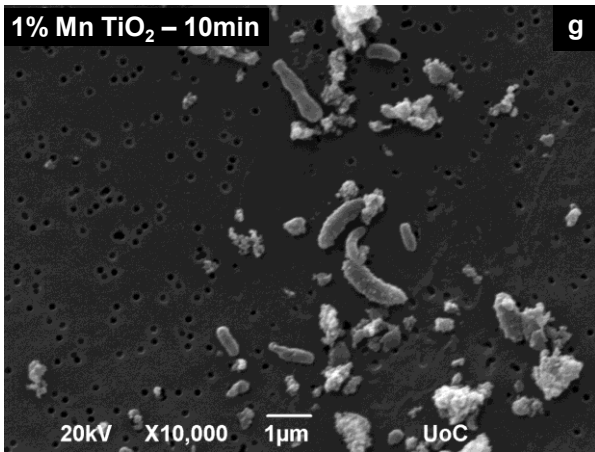


526

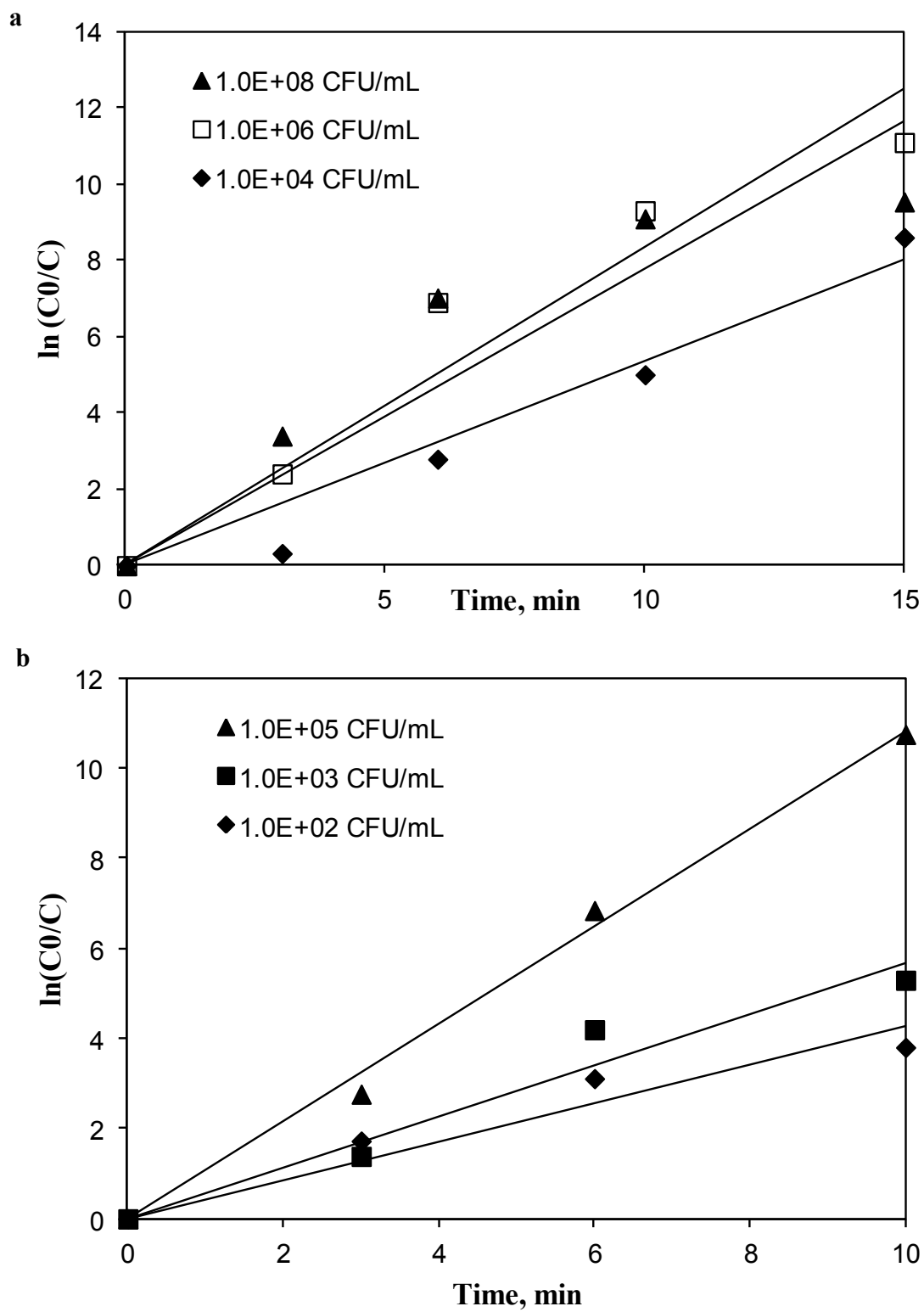
527







531 **Figure 8**



532

533

